RSC Advances

PAPER

View Article Online
View Journal | View Issue

Cite this: *RSC Adv.*, 2021, **11**, 33646

Nitrogen doped carbon for Pd-catalyzed hydropurification of crude terephthalic acid: roles of nitrogen species†

Limin He,[a] Yangdong Wang,[a] Huanxin Gao,[a] Zhicheng Liu*[a] and Zaiku Xie *[b]

The purification of crude terephthalic acid was performed by the hydrogenation of 4-carboxybenzaldehyde (4-CBA) over activated carbon (AC) supported Pd catalysts in industry. However, traditional Pd/AC catalysts usually suffer from low hydrogenation activity and poor thermal stability. Herein, nitrogen was incorporated into AC *via* a simple hydrothermal treatment of AC with urea as the nitrogen resource. The N doped AC contained pyridinic N, pyrrolic N, graphitic N and oxidized N. Wide characterizations revealed that N doping not only effectively improved the dispersion of Pd NPs but also increased the proportion of Pd^0. In addition, N doping also enhanced the dissociative adsorption capacity of molecular hydrogen. More importantly, the resistance to sintering of Pd NPs was efficiently suppressed after N doping. As a result, N doped AC supported Pd showed both higher activity and better thermal stability than the N-free one.

Received 27th August 2021
Accepted 28th September 2021

DOI: 10.1039/d1ra06479g

rsc.li/rsc-advances

1. Introduction

Purified terephthalic acid (PTA) is an important intermediate used for the production of polyesters. Industrially, the crude terephthalic acid (CTA) is produced by the oxidation of *p*-xylene (PX) over a homogeneous catalyst, containing a small amount of by-product 4-carboxybenzaldehyde (4-CBA). The removal of 4-CBA is generally carried out over Pd catalysts in a trickle reactor under a hydrogen atmosphere. Among the catalyst supports used (TiO_2, SiC, SiO_2 *etc.*),[1–4] activated carbon (AC) supported Pd catalysts are still considered as one of the most efficient catalysts for the hydrogenation of 4-CBA.[5,6] However, there are some drawbacks of traditional Pd/AC. Firstly, Pd nanoparticles (NPs) tend to aggregate due to the weak interaction of Pd and AC under reaction conditions, resulting in limited stability and life time of Pd/AC.[7,8] Secondly, Pd is a noble metal and has high cost. Pd/AC needs to be optimized in order to maximize hydrogenation activity with the viewpoint of maximum atom efficiency of noble metal catalysts as well as sustainable development. Studies have shown that surface chemical and structural properties of a catalyst support can modulate catalytic performance of heterogeneous catalysts by changing the morphology or electronic structure of the deposited metal nanoparticles.[9–11] For instance, CNTs oxidized with HNO_3/H_2SO_4 can functionalize CNTs with surface oxygen groups and strengthen the coordination of Pt with surface oxygen groups, resulting in highly dispersed Pt NPs.[12] Hence, surface modification of AC was one effective approach to modify Pd catalysts with improved catalytic activity and good stability.

Recent studies indicated that N doping of carbon materials can reinforce the interaction between metal and the carbon support.[13–16] N doping into carbon materials as supports had profound impact on electronic structures of metal NPs, such as Ni,[17] Pt,[18] Pd,[19] Ru[20] and Co[21] based catalysts, which was beneficial for their catalytic activity and stability. However, the relations of metallic NPs and nitrogen species resulting in excellent catalytic behavior were complicated. The electronegative property of N atoms may increase the electron density of metal NPs, resulting in the electron transfer from N to metal NPs. Ning *et al.* demonstrated that the binding energy of Pt^0 of Pt/NCNTs shifted to the low binding energy side compared with Pt/CNTs.[22] In addition, N doping can greatly improve metal NPs dispersion and in turn contributed to better catalytic activity.[23–25] N doping was also helpful for the stabilization of metal NPs and further improve the stability of supported metal catalysts.[26–28] Until now, N doped carbon materials supported metal catalysts for the hydrogenation of 4-CBA remained less exploration and large challenge.

Here, nitrogen was doped into AC *via* the hydrothermal method with urea as nitrogen resource. Then, the obtained N doped AC was used as a support for the loading of Pd NPs by a wetness impregnation method. After N doping, Pd catalyst exhibited higher catalytic activity and better thermal stability for the hydrogenation of 4-CBA compared with un-doped one. Furthermore, the influence of N species on structure properties

[a]*State Key Laboratory of Green Chemical Engineering and Industrial Catalysis, Shanghai Research Institute of Petrochemical Technology, SINOPEC Corp., Shanghai 201208, China. E-mail: liuzc.sshy@sinopec.com*

[b]*China Petrochemical Corporation (SINOPEC Group), Beijing 100728, China. E-mail: xzk@sinopec.com*

† Electronic supplementary information (ESI) available. See DOI: 10.1039/d1ra06479g

of Pd catalysts and their effects on catalytic performance were discussed in detail.

2. Experimental section

2.1 Materials

Palladium chloride was purchased from Sigma-Aldrich. 4-CBA were purchased from Aladdin Chemical Reagent (Shanghai, China). Activated carbon was supplied by Sinopec Shanghai Petrochemical Company Limited. Phosphoric acid (H_3PO_4, 85 wt% in H_2O), and ammonia solution ($NH_3 \cdot H_2O$, 25 wt% in H_2O) were purchased from Sinopharm Chemical Reagent Co., Ltd. All other chemicals were analytical grade and used without further purification.

2.2 Preparation of N doped AC

The N doped activated carbon was synthesized by a hydrothermal process using urea as the nitrogen resource. Typically, 0.6 g activated carbon was dispersed in 5 M urea solution. Then, the mixture solution was transferred to a 200 ml Teflon-lined autoclave and heated at 180 °C for 4 h. After reaction, the autoclave was cooled down to room temperature. Then, the product was collected by filtration and washed using de-ionized water. After dried at 120 °C, the sample was calcined at 500 °C for 3 h in nitrogen atmosphere. The final sample was abbreviated as N_AC.

2.3 Preparation of Pd supported N doped AC

The Pd supported N doped AC were prepared by impregnating N doped AC with H_2PdCl_4 aqueous solution and sodium citrate as the stabilizing agent. After impregnation, 10 ml of 0.1 M $NaBH_4$ aqueous as reductive agent was added dropwise to the above solution under vigorous stirring for 1 h. Finally the Pd catalyst was obtained by filtration, washing with water and dried at 120 °C. The obtained samples were denoted as Pd/N_AC. For comparison, Pd supported on N-free AC was also prepared by the same above method, and denoted as Pd/AC. The loading amount of Pd was 0.5 wt% for all Pd catalysts.

2.4 Catalyst characterization

Powder X-ray diffraction (XRD) measurement was performed using Bruker D8 Advance diffractometer, with Cu Kα radiation ($g = 0.15406$ nm) at step scan 0.02° from 5° to 80°. The nitrogen adsorption/desorption isotherms were measured at 77 K on a Micromeritics ASAP 2020 analyzer. The total porous volume (V_{total}) was estimated from the adsorbed capacity of nitrogen at a relative pressure P/P_0 of 0.98 whereas the microporous volume (V_{micro}) was determined using the *t*-plot method. The morphology and microstructure were measured by scanning electron microscopy (FE-SEM, Hitachi S-4800). X-ray photoelectron spectroscopy (XPS) was carried out with an AXIS Ultra DLD photoelectron spectrometer (Kratos Analytical, UK) using monochromatic Al Kα radiation. The C 1s with the binding energy of 284.6 eV was applied as reference to calibrate the position of the other peaks. The hydrogen temperature programmed desorption (H_2-TPD) experiments was conducted using a Micromeritics Autochem II 2920 instrument equipped with a thermal conductivity detector (TCD). Prior to the tests, the samples are pretreated under hydrogen atmosphere at 200 °C for 60 min. H_2 desorption in Ar flow was started with temperature ramping from 50 °C to 800 °C. Palladium dispersion on *xx* was determined by hydrogen titration of chemisorbed oxygen (H_2–O_2 titration) in a Micromeritics Autochem II 2920 instrument with a thermal conductivity detector (TCD). Prior to the tests, 400 mg Pd catalysts were first reduced at 200 °C under a hydrogen atmosphere for 120 min; hydrogen absorbed on the surface of catalyst was titrated by 15 pulses of oxygen until full saturation; then the resulting monolayer of adsorbed oxygen was titrated using 15 pulses of hydrogen until constant TCD signal detected. In addition, TEM images of Pd catalysts were performed on a Tecnai 20 S-TWIN electron microscope operated at 200 kV. The content of Pd loading was determined by an inductively coupled plasma emission spectrometer (ICP-OES, Varian 725 ES). The bulk elemental composition (C, H, N) was determined by using an elemental analyzer (SDCHN435, Hunan Sundy, China).

2.5 Catalytic activity tests

The catalytic hydrogenation of 4-CBA was carried out in a 100 ml stainless-steel autoclave. In a typical test, 0.15 g of 4-CBA, 50 mg catalyst with 20–40 mesh and 50 ml of de-ionized water were placed in the autoclave and mixed together. After sealed, the autoclave was pressured with 0.8 MPa hydrogen, then heated to 80 °C in a water bath. After reaction, the obtained liquid samples were treated with 14% $NH_3 \cdot H_2O$ and 17% H_3PO_4 aqueous solutions respectively. Finally, the liquid products were analyzed using high-performance liquid chromatography (HPLC, Agilent 1200) equipped with a UV detector and a C-18 column (4.6 × 250 mm, 5 μm) (Scheme 1).

3. Results and discussion

3.1 The textural properties of Pd catalysts

The influence of N doping and Pd loading on the porous structure of AC has been investigated by N_2 physical adsorption–desorption at 77 K. The type I isotherm curves indicated the nature of microstructure of activated carbon materials (Fig. S1†). The porosity parameters were summarized in Table 1. Compared with AC, N_AC showed a slight increase in BET area and pore volume after N doping. The hydrothermal treatment of activated carbon at high temperature of water facilitated the production of porous structure.[29,30] Compared with supports, the slight decrease of surface area of Pd/AC and Pd/N_AC

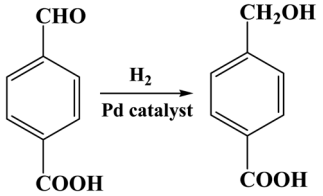

Scheme 1 Hydrogenation pathway of 4-CBA over Pd catalysts.

Table 1 Summary of porosity parameters of supports and Pd catalysts

Sample	S_{BET} (m^2 g^{-1})	S_{mic} (m^2 g^{-1})	V_{total} (cm^3 g^{-1})	V_{mic} (cm^3 g^{-1})
AC	991.7	836.8	0.482	0.383
Pd/AC	910.4	770.9	0.439	0.352
N_AC	1023.8	844.7	0.497	0.385
Pd/N_AC	925.0	765.4	0.445	0.348

indicated that part of surface sites of supports were occupied by dispersed Pd NPs after Pd loading.

3.2 The electronic structures of N and Pd

The direct evidence of N doping was provided by XPS, and the N 1s spectra of N_AC and Pd/N_AC were shown in Fig. S2.† The high resolution C 1s spectra of N_AC and Pd/N_AC can be deconvoluted into three peaks, corresponding to C=C (284.6 eV), C–N (285.5 eV) and O–C=O (288.9 eV) respectively.[31–33] These results indicated the incorporation of N atoms into carbon skeleton. The high resolution N 1s XPS spectra of AC and Pd/N_AC (Fig. 1c and d) further indicated the four forms of heteroatom N in the carbon. The four kinds of nitrogen species appeared at different binding energies, corresponding to pyridinic N, pyrrolic N, graphitic N and oxidized N, respectively. After Pd loading, the total nitrogen content decreased from 1.34 at% to 1.12 at% (Fig. S3†). Furthermore, the content of four different nitrogen species before and after Pd loading were summarized in Fig. 2. The relative percentages of pyridinic N, pyrrolic N, graphitic N have no obvious changes except of the slight decreasing of oxidized N. Moreover, the elemental analysis results further revealed that the total N content was similar before (0.58 wt%) and after (0.53 wt%) Pd loading (Table S1†).

To further understand the important influence of N doping on electronic structure of Pd catalysts, XPS was carried out to

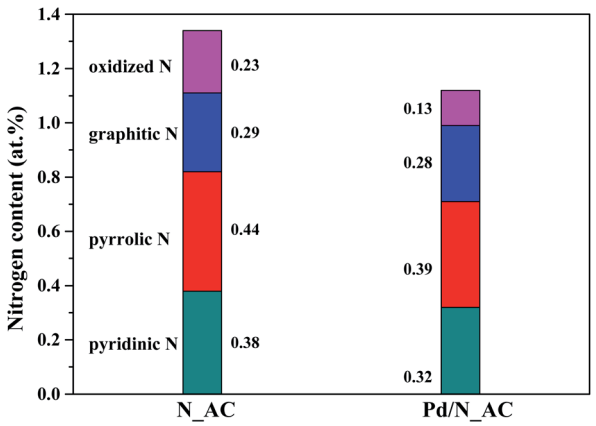

Fig. 2 Different N species distribution of N_AC and Pd/N_AC.

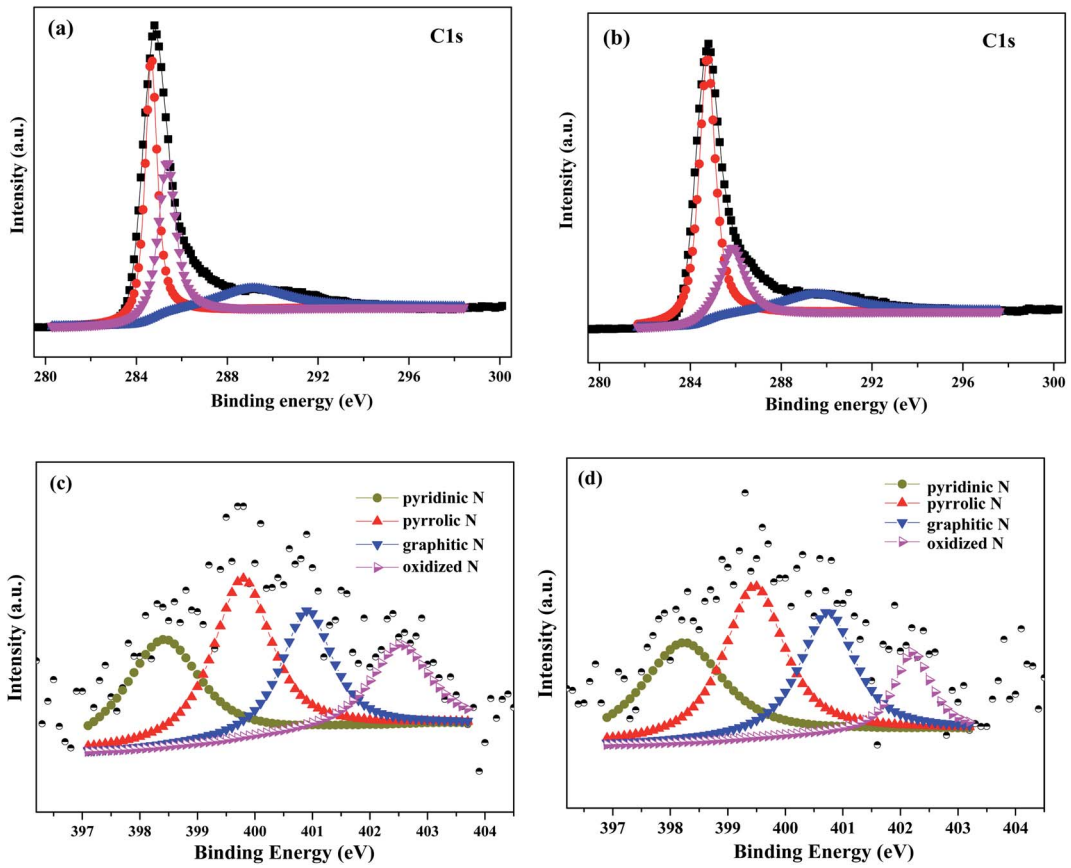

Fig. 1 C 1s and N 1s XPS spectra of (a and c) N_AC and (b and d) Pd/N_AC.

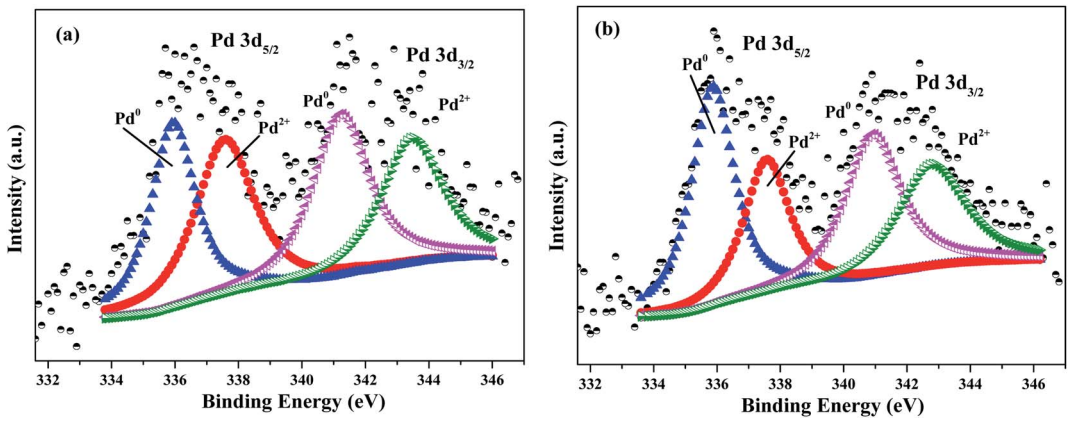

Fig. 3 Pd 3d XPS spectra of (a) Pd/AC and (b) Pd/N_AC.

investigate chemical state of Pd. As shown in Fig. 3, the surface chemical state of Pd species consisted of oxidation state Pd (Pd^{2+}) and metallic state Pd (Pd^0). According to XPS analysis, the ratio of Pd^0/Pd^{2+} in Pd/AC and Pd/N_AC was 1.04 and 1.32, respectively. These results clearly indicated that N doping favored the formation of Pd^0. Since pyridinic N and pyrrolic N possessed lone pair of electrons, N species can provide an electron-enriched microenvironment and finally can increase the content of Pd^0 by donating its electron to Pd.[34] Therefore, N dopants can serve as metal coordination sites for anchoring Pd. Wang *et al.* also revealed that N in carbon texture was beneficial for stabilizing Pd^0 and preventing the reoxidation of metallic Pd.[35]

3.3 The dispersion of Pd nanoparticles

The typical HRTEM images of Pd catalysts without and with N doping were shown in Fig. 4. The Pd particle size distribution showed that the N-doped Pd catalyst had narrow diameter distribution with smaller size of Pd NPs than that of the N-free catalyst. This result indicated that N_AC was an ideal support for stabilizing Pd NPs. Pd dispersion before and after N doping have been further tested by hydrogen-oxidation titration and the results were summarized in Table 2. The actual Pd loading were also tested by ICP analysis, which was close to the theoretical value. After N doping, Pd dispersion increased to 35.7% compared with that of the N-free sample (22.4%). Surface nitrogen-containing groups such as pyridinic N and pyrrolic N have been confirmed to increase metal dispersion (*e.g.* Pt, Ni) *via* strong metal–N bond at the interface.[26,27,36] In recent years, atomically dispersed metal catalysts in N doped graphene matrix were also successfully synthesized with wide applications.[37–39] Therefore, nitrogen doping in carbon materials held promising potential for stabilizing highly dispersed metal nanoparticles.[40,41]

3.4 Activation of hydrogen molecular

As reported, the dissociatively adsorption ability of hydrogen molecular were closely associated with catalytic activities of Pd catalysts. Here, hydrogen activation ability over Pd catalysts were detected by H_2-TPD. As shown in Fig. 5, Pd catalysts before and after N doping showed a low temperature desorption peak below 100 °C, which was attributed to the desorption of weak adsorbed hydrogen molecular. The large desorption peaks at high temperature (275 °C for Pd/AC and 301 °C for Pd/N_AC) were ascribed to the desorption of strongly adsorbed hydrogen species. The higher desorption temperature in Pd/N_AC indicated the strengthening Pd–support interactions due to N doping. In addition, the intensity of desorption peak in

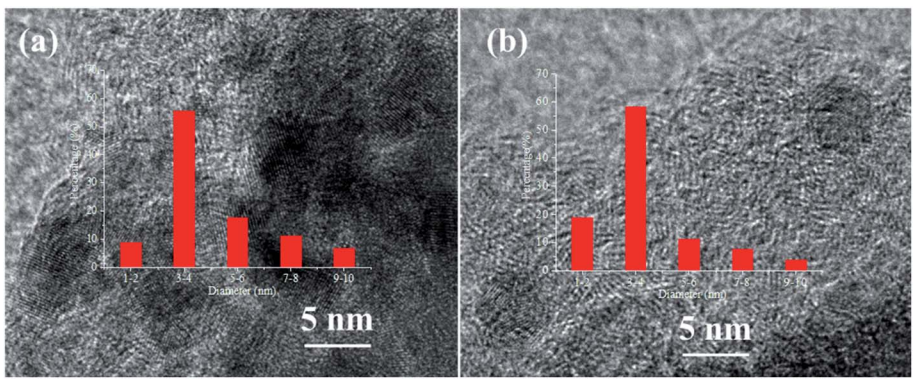

Fig. 4 HRTEM images and size distribution of (a) Pd/AC and (b) Pd/N_AC.

Table 2 Physical–chemical properties of Pd catalysts before and after N doping

Entry	Catalyst	Pd loading[a] (wt%)	Metal dispersion[b] (%)
1	Pd/AC	0.47	22.4
2	Pd/N_AC	0.48	35.7

[a] Determined by ICP-AES. [b] Determined by H_2–O_2 titration.

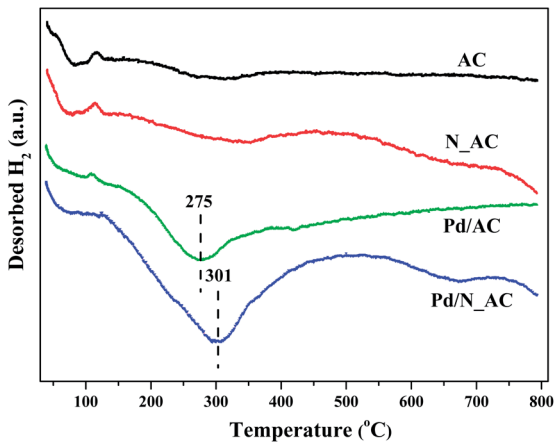

Fig. 5 H_2-TPD profiles of AC, N_AC, Pd/AC and Pd/N_AC.

Pd/N_AC was obviously stronger than that in Pd/AC, suggesting the doping of N atoms into AC facilitated the adsorption and activation of molecular hydrogen. Rossi *et al.* illustrated the crucial role of nitrogen atoms over Au@N-doped carbon catalysts in promoting the heterolytic activation of molecular hydrogen.[42]

3.5 Stability of Pd catalysts

To better understand the crucial role of N species, the sintering resistance of Pd catalysts was investigated by XRD (Fig. 6). The catalysts were calcined in N_2 at 500 °C. Compared with fresh Pd catalysts (Fig. S5†), the intensity of Pd (111) diffraction peaks obviously increased after heat treatment at 500 °C. The particle sizes of Pd NPs were calculated through Scherrer equation. The average size of Pd NPs in Pd/N_AC was 14.8 nm which was smaller than that of Pd/C (16.7 nm). This results indicated that N doping can secure Pd NPs on their original position and inhibit the growth of Pd NPs.[43,44] In addition, the surface area of Pd/AC-500 and Pd/N_AC-500 was 921.2 and 940.6 $m^2\ g^{-1}$, and the corresponding pore volume was 0.488 and 0.489 $cm^3\ g^{-1}$ respectively. The surface area and pore volume of aged samples slightly increased compared with the fresh ones.

3.6 Influence of nitrogen species on catalytic performance of Pd catalysts

The activities of Pd catalysts before and after N doping were tested for the hydrogenation of 4-CBA. When N_AC without Pd used as the catalyst, the conversion of 4-CAB was extremely low, suggesting the N_AC was inactive due to its poor ability for hydrogen molecular activation. Generally, metal state Pd^0 was catalytic active center of hydrogenation reaction.[45,46] As shown in Fig. 7, Pd loaded on N_AC exhibited higher catalytic activity than that on N-free AC. After reaction for 3 h, the conversion of 4-CBA reached 91.5% while the conversion of Pd/AC was only 83.4%. After reaction for 3 h, the contents of Pd over Pd/AC and Pd/N_AC catalysts were analyzed *via* ICP, and they were 0.47% and 0.48% respectively. Therefore, Pd leaching was negligible. The above structure characterizations indicated N-functionalization of AC played important roles in the hydrogenation of 4-CBA. Firstly, N species as electron donors in support could affect the chemical state of Pd NPs. N doping increased the content of Pd^0 due to the strong electron donating effect of N species. In addition, nitrogen species promoted activation capacity of hydrogen molecular, which was beneficial for the hydrogenation reaction. More importantly, N species enhanced the superior dispersion of Pd NPs with narrow size distribution. Thus, the improved activity of Pd/N_AC could be attributed to the strong coordination of Pd with N species.

In present work, N doped AC samples were synthesized by a hydrothermal method with urea as nitrogen resource. Fig. S6† showed the catalytic activity of hydrogenation of 4-CBA over Pd catalysts with different N doped AC as supports. The N doping

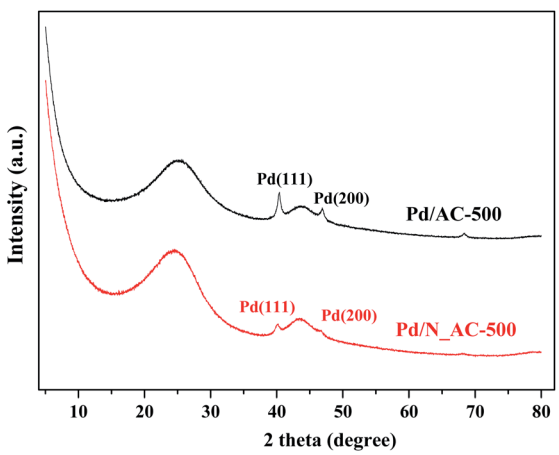

Fig. 6 XRD patterns of Pd catalysts after calcined at 500 °C.

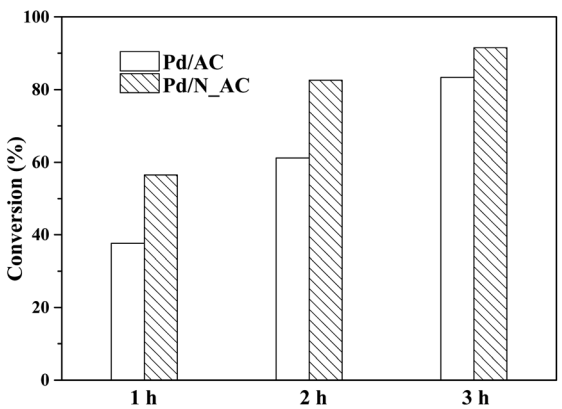

Fig. 7 Catalytic activity of Pd catalysts for 4-CBA hydrogenation.

was indeed beneficial for the hydrogenation of 4-CBA compared with N-free AC supported Pd. Here, N doped AC synthesized at 180 °C for 4 h supported Pd catalyst exhibited the best activity.

4. Conclusions

In summary, nitrogen heteroatoms were incorporated into AC by a simple hydrothermal method with urea as nitrogen resource. Pd supported on different N doped AC were prepared by a wetness impregnation method and their catalytic performances were evaluated in the hydrogenation of 4-CBA under mild reaction conditions. After N doping, Pd catalysts exhibited enhanced catalytic activity compared with Pd/AC. The critical roles of N dopant in influencing the electronic structures of Pd on Pd/N_AC were investigated. Firstly, the XPS spectra verified that N species as electron donor can increase the electron density of Pd NPs, thus keeping the high percentage of Pd^0 in Pd/N_AC. Secondly, H_2-TPD tests revealed that N doping enhanced the activation ability of hydrogen molecular over Pd/N_AC, and thereby facilitated the hydrogenation activity of 4-CBA. Thirdly, Pd dispersion increased to 35.7% after N doping, and facilitated catalytic hydrogenation reaction performance. More importantly, N doping promoted the effective immobilization of Pd NPs by strong metal–support interaction through the large electron affinity of N. As a result, Pd/N_AC showed a better sintering resistance of Pd NPs than Pd/AC. The present work may offer a feasible strategy to synthesize other metal catalysts with high dispersion and well thermal stability.

Conflicts of interest

There are no conflicts to declare.

Acknowledgements

We gratefully acknowledged the financial support from the National Natural Science Foundation of China (U1663221).

Notes and references

1 S. H. Jhung, A. V. Romanenko, K. H. Lee, Y. S. Park, E. M. Moroz and V. A. Likholobov, *Appl. Catal., A*, 2002, **225**, 131–139.
2 K. T. Li, M. H. Hsu and I. Wang, *Catal. Commun.*, 2008, **9**, 2257–2260.
3 Y. H. Zhou, X. Y. Li, X. L. Pan and X. H. Bao, *J. Mater. Chem.*, 2012, **22**, 14155–14159.
4 Z. Li, C. Wang, X. Chen, X. Wang, X. Li, Y. Yamauchi, X. Xu, J. Wang, C. Lin, D. Luo, X. Wang and X. S. Zhao, *Chem. Eng. J.*, 2020, **381**, 122588.
5 F. Menegazzo, T. Fantinel, M. Signoretto and F. Pinna, *Catal. Commun.*, 2007, **8**, 876–879.
6 X. Li, K. Tie, Z. Li, Y. Guo, Z. Liu, X. Liu, X. Liu, H. Feng and X. S. Zhao, *Appl. Surf. Sci.*, 2018, **447**, 57–62.
7 R. Pellegrini, G. Agostini, E. Groppo, A. Piovano, G. Leofanti and C. Lamberti, *J. Catal.*, 2011, **280**, 150–160.
8 S. Tourani, F. Khorasheh, A. M. Rashidi and A. A. Safekordi, *J. Ind. Eng. Chem.*, 2015, **28**, 202–210.
9 S. S. Rich, J. J. Burk, C. S. Kong, C. D. Cooper, D. E. Morse and S. K. Buratto, *Carbon*, 2015, **81**, 115–123.
10 Y. X. Tuo, L. J. Shi, H. Y. Cheng, Y. A. Zhu, M. L. Yang, J. Xu, Y. F. Han, P. Li and W. K. Yuan, Insight into the support effect on the particle size effect of Pt/C catalysts in dehydrogenation, *J. Catal.*, 2018, **360**, 175–186.
11 S. Kattel, W. Yu, X. Yang, B. Yan, Y. Huang, W. Wan, P. Liu and J. G. Chen, *Angew. Chem., Int. Ed.*, 2016, **55**, 7968–7973.
12 R. V. Hull, L. Li, Y. Xing and C. C. Chusuei, *Chem. Mater.*, 2006, **18**, 1780–1788.
13 H. Wang, T. Maiyalagan and X. Wang, *ACS Catal.*, 2012, **2**, 781–794.
14 M. Li, F. Xu, H. Li and Y. Wang, *Catal. Sci. Technol.*, 2016, **6**, 3670–3693.
15 Y. Cao, S. Mao, M. Li, Y. Chen and Y. Wang, *ACS Catal.*, 2017, **7**, 8090–8112.
16 X. Y. Li, X. L. Pan, Y. H. Zhou and X. H. Bao, *Carbon*, 2013, **57**, 34–41.
17 R. Nie, H. Yang, H. Zhang, X. Yu, X. Lu, D. Zhou and Q. Xia, *Green Chem.*, 2017, **19**, 3126–3134.
18 G. Wu, D. Li, C. Dai, D. Wang and N. Li, *Langmuir*, 2008, **24**, 3566–3575.
19 R. Nie, H. Jiang, X. Lu, D. Zhou and Q. Xia, *Catal. Sci. Technol.*, 2016, **6**, 1913–1920.
20 Y. Cao, L. Ding, Z. Qiu and H. Zhang, *Catal. Commun.*, 2020, **143**, 106048.
21 F. A. Westerhaus, R. V. Jagadeesh, G. Wienhofer, M. M. Pohl, J. Radnik, A. E. Surkus, J. Rabeah, K. Junge, H. Junge, M. Nielsen, A. Bruckner and M. Beller, *Nat. Chem.*, 2013, **5**, 537–543.
22 X. Ning, H. Yu, F. Peng and H. Wang, *J. Catal.*, 2015, **325**, 136–144.
23 W. Qian, L. Lin, Y. Qiao, X. Zhao, Z. Xu, H. Gong, D. Li, M. Chen, R. Huang and Z. Hou, *Appl. Catal., A*, 2019, **585**, 117183.
24 Y. Dai, C. Jiang, M. Xu, B. Bian, D. Lu and Y. Yang, *Appl. Catal., A*, 2019, **580**, 158–166.
25 C. Pu, J. Zhang, G. Chang, Y. Xiao, X. Ma, J. Wu, T. Luo, K. Huang, S. Ke, J. Li and X. Yang, *Carbon*, 2020, **159**, 451–460.
26 T. Wang, Z. Dong, T. Fu, Y. Zhao, T. Wang, Y. Wang, Y. Chen, B. Han and W. Ding, *Chem. Commun.*, 2015, **51**, 17712–17715.
27 L. Perini, C. Durante, M. Favaro, V. Perazzolo, S. Agnoli, O. Schneider, G. Granozzi and A. Gennaro, *ACS Appl. Mater. Interfaces*, 2015, **7**, 1170–1179.
28 S. Li, Y. Shi, J. Zhang, Y. Wang, H. Wang and J. Lu, *ChemSusChem*, 2021, **14**, 2050–2055.
29 L. Sun, L. Wang, C. Tian, T. Tan, Y. Xie, K. Shi, M. Li and H. Fu, *RSC Adv.*, 2012, **2**, 4498.
30 R. Shi, J. Zhao, S. Liu, W. Sun, H. Li, P. Hao, Z. Li and J. Ren, *Carbon*, 2018, **130**, 185–195.
31 C. Zhang, L. Fu, N. Liu, M. Liu, Y. Wang and Z. Liu, *Adv. Mater.*, 2011, **23**, 1020–1024.

32 W. Ding, L. Li, K. Xiong, Y. Wang, W. Li, Y. Nie, S. Chen, X. Qi and Z. Wei, *J. Am. Chem. Soc.*, 2015, **137**, 5414–5420.
33 H. Sun, Y. Zhu, B. Yang, Y. Wang, Y. Wu and J. Du, *J. Mater. Chem. A*, 2016, **4**, 12088–12097.
34 Y. Wang, J. Yao, H. Li, D. Su and M. Antonietti, *J. Am. Chem. Soc.*, 2011, **133**, 2362–2365.
35 X. Xu, Y. Li, Y. Gong, P. Zhang, H. Li and Y. Wang, *J. Am. Chem. Soc.*, 2012, **134**, 16987–16990.
36 D. He, Y. Jiang, H. Lv, M. Pan and S. Mu, *Appl. Catal., B*, 2013, **132–133**, 379–388.
37 H. Fei, J. Dong, M. J. Arellano-Jimenez, G. Ye, N. Dong Kim, E. L. Samuel, Z. Peng, Z. Zhu, F. Qin, J. Bao, M. J. Yacaman, P. M. Ajayan, D. Chen and J. M. Tour, *Nat. Commun.*, 2015, **6**, 8668.
38 H. B. Yang, S. F. Hung, S. Liu, K. Yuan, S. Miao, L. Zhang, X. Huang, H. Y. Wang, W. Cai, R. Chen, J. Gao, X. Yang, W. Chen, Y. Huang, H. M. Chen, C. M. Li, T. Zhang and B. Liu, *Nat. Energy*, 2018, **3**, 140–147.
39 T. Zhang, X. Han, A. Han, Y. Li, J. Liu, T. Zhang, H. Yang, B. Liu, E. Hu, X. Q. Yang and L. Wang, *Angew. Chem., Int. Ed.*, 2020, **59**, 12055–12061.
40 G. Sun, Z. J. Zhao, R. Mu, S. Zha, L. Li, S. Chen, K. Zang, J. Luo, Z. Li, S. C. Purdy, A. J. Kropf, J. T. Miller, L. Zeng and J. Gong, *Nat. Commun.*, 2018, **9**, 4454.
41 H. Yu, L. Zhang, S. Gao, H. Wang, Z. He, Y. Xu and K. Huang, *J. Catal.*, 2021, **396**, 342–350.
42 J. L. Fiorio, R. V. Gonçalves, E. Teixeira-Neto, M. A. Ortuño, N. López and L. M. Rossi, *ACS Catal.*, 2018, **8**, 3516–3524.
43 Z. Li, J. Liu, C. Xia and F. Li, *ACS Catal.*, 2013, **3**, 2440–2448.
44 K. Zhang, Q. Meng, H. Wu, T. Yuan, S. Han, J. Zhai, B. Zheng, C. Xu, W. Wu, M. He and B. Han, *Green Chem.*, 2021, **23**, 1621–1627.
45 Z. Z. Wei, Y. T. Gong, T. Y. Xiong, P. F. Zhang, H. R. Li and Y. Wang, *Catal. Sci. Technol.*, 2015, **5**, 397–404.
46 A. Nagendiran, V. Pascanu, A. Bermejo Gomez, G. Gonzalez Miera, C. W. Tai, O. Verho, B. Martin-Matute and J. E. Backvall, *Chem.–Eur. J.*, 2016, **22**, 7184–7189.